Water Science and Engineering 2022, 15(1): 69−77

HOSTED BY

ELSEVIER

Available online at www.sciencedirect.com

Water Science and Engineering

journal homepage: wse.hhu.edu.cn

Monopile responses to monotonic and cyclic loading in undrained sand using 3D FE with SANISAND-MSu

Hao-yuan Liu [a], Amir M. Kaynia [b,c,*]

[a] *Norwegian Geotechnical Institute, Oslo 0806, Norway*
[b] *Norwegian University of Science and Technology, Trondheim 7491, Norway*
[c] *Norconsult, Sandvika 1338, Norway*

Received 30 June 2021; accepted 1 September 2021
Available online 9 December 2021

Abstract

Monopile response under undrained conditions in sand is gaining increasing interests owing to the recent development of offshore wind farms in seismic regions. Pore pressure evolution in liquefiable soil can significantly reduce the strength and stiffness of the soil which in turn affects the structural dynamic response. Several numerical models have been developed in the last two decades to enhance understanding of the mechanism of monopile−soil interaction with the existence of pore water pressure. In this study, the effects of geometry and static vertical load on monopile lateral response were studied using three-dimensional finite element methods that consider the existence of lateral cyclic load-induced pore water pressure. To achieve reliable simulation results of pore pressure development and pile displacement accumulation during cyclic loading, the simple anisotropic sand model with memory surface for undrained cyclic behavior of sand was adopted. For piles with the same diameter, a accumulated pile head displacement during lateral cyclic loading decreased linearly with increasing pile embedded length but increased with increasing eccentricity. Static vertical load had minor effects on pile cyclic lateral response. The distributions of mean effective stress and pore water pressure in the soil domain were presented. The pile reaction curve (cyclic soil reaction against pile defection) of the monopile was extracted. The numerical results aim to provide reference for optimized engineering design procedures.
© 2021 Hohai University. Production and hosting by Elsevier B.V. This is an open access article under the CC BY-NC-ND license (http://creativecommons.org/licenses/by-nc-nd/4.0/).

Keywords: Offshore monopile; Pore pressure; Cyclic loading; Soil−structure interaction; Sand

1. Introduction

Different renewable energy solutions have been proposed and adopted to meet the global reduction target for greenhouse gas emission. Among them, offshore wind energy industry is rapidly developing for reasons including less negative impact on ecological system, more stable wind supply, and higher wind speed (Kaynia, 2019).

Currently, the majority of offshore wind turbine (OWT) foundations are monopiles that are large-diameter tubular steel piles. Typical OWTs with a capacity of around 5 MW have monopile diameters of around 4−6 m and are located up to 20−30 km from shore and in water depths of up to 30 m. Offshore monopiles generally experience cyclic loading induced by wind, waves, and currents. Recent development of technologies as well as the requirements from industry have promoted OWT monopiles to move towards farther and deeper waters with even larger pile diameters. In some recent projects, OWTs have been designed with diameters exceeding 10 m. This naturally rises to the problems such as harsher environmental loading and thus more challenging design criteria. Achieving cost-optimization targets in offshore monopile design and construction reveals the importance of comprehensive understanding of monopile behavior under varying loading and soil drainage conditions.

* Corresponding author.
E-mail address: amir.kaynia@ntnu.no (Amir M. Kaynia).
Peer review under responsibility of Hohai University.

https://doi.org/10.1016/j.wse.2021.12.001
1674-2370/© 2021 Hohai University. Production and hosting by Elsevier B.V. This is an open access article under the CC BY-NC-ND license (http://creativecommons.org/licenses/by-nc-nd/4.0/).

In design practice, the monopile behavior under long-term cyclic loading in a sand domain is commonly assumed drained (API, 2014). However, the accuracy of such an assumption is questionable especially when high-intensity dynamic cyclic loading (for instance, earthquake shaking) is applied (Esfeh and Kaynia, 2020). During such events, one of the essential differences of soil behavior is the increase in pore water pressure, compared to the soil behavior under fully drained conditions. Generally, the accumulation of pore water pressure in saturated soil affects soil stiffness and strength. Such effects strongly impact monopile global dynamic behavior, as well as monopile tilting (Jostad et al., 2020; Liu and Kaynia, 2021).

As more offshore wind farms are planned/constructed in liquefiable soil sites, monopile behavior under different soil drainage conditions needs critical assessment. Many efforts from experimental perspective have been devoted for such a purpose, spanning from small-scale single gravity tests (LeBlanc et al., 2010; Richards et al., 2020) to centrifuge tests (Klinkvort, 2013; Truong et al., 2019). However, due to the practical difficulties in test design and restrictions from test equipment, most experimental works have been limited to dry or fully drained load conditions.

Numerical approach is a practical alternative. In this category, the macro-element modeling method (Houlsby et al., 2017; Page et al., 2019) and $p-y$ (where p indicates the soil reaction and y is the pile deflection) modeling method have gained broad popularity for reasons of simplicity in concept and relatively short computation time. In addition, a three-dimensional (3D) finite element (FE) analysis incorporating an explicit constitutive model is also a common simulation approach when reliable empirical relationships or comprehensive experimental data for estimating long-term cyclic behavior of soil are available (Staubach and Wichtmann, 2020).

Apart from the numerical methods listed above, the implicit 3D FE analysis method (Niemunis et al., 2005) is also commonly used, especially in the academia (Liu et al., 2021; Tasiopoulou et al., 2021). In this category, each loading cycle is simulated by many sub-loading steps, leading to long computational time when such analyses are performed. Meanwhile, the accuracy of implicit 3D FE simulation results depends highly on the accuracy of the used constitutive models. Despite these limitations, the implicit 3D FE method is gaining wider attention nowadays in the offshore geotechnical community, due to its high potential to link the local soil response to the global foundation performance.

Numerous implicit cyclic constitutive models for sand have been developed during past decades. Many of them are based on elasto-plasticity theory. Constitutive models adopting bounding surface plasticity (Dafalias and Popov, 1975; Krieg, 1975) and multi-surface plasticity (Mróz, 1967) stand out and are well accepted owing to the relatively simple conceptual configuration but good simulation performance. A currently well-acknowledged sand cyclic model belonging to bounding surface plasticity is the simple anisotropic sand (SANISAND) model proposed by Dafalias and Manzari (2004) (referred to as SANISAND2004 in this work). In this model, inherent fabric effects on sand's post-dilation behavior are accounted for through the fabric tensor in its flow rule. Such an attempt has raised wide attention to including soil fabric effects in constitutive formulating. Many SANISAND-based constitutive models have been developed since the initial development. Liu et al. (2019) introduced the memory surface (MS) concept into the SANISAND framework (referred to as SANISAND-MS) to simulate the fabric effects throughout the plastic straining period by modifying the hardening rule and flow rule of the model. The strategy showed great improvement in predicting soil drained ratcheting performance (Liu and Pisanò, 2019). Further, Liu et al. (2020) included the fabric evolution history and stress ratio effects in SANISAND-MS to better capture the cyclic behavior of sand under undrained response.

In this work, the implicit 3D FE method was selected to study the response of offshore monopiles under undrained conditions. The bounding surface SANISAND-MS model that caters to undrained cyclic behavior of sand (Liu et al., 2020) was adopted in this study (hereafter referred to as SANISAND-MSu). Pore water pressure effects were highlighted by comparing monopile response under drained and undrained conditions. Effects of monopile geometry, characterized through L/D and e/D ratios (where L, D, and e are the pile embedded length, monopile outer diameter, and load eccentricity, respectively), were studied. The presence of static vertical load, namely the weight of the tower and turbine, on the cyclic lateral capacity of pile was also investigated. This work aimed to contribute to the development of optimized design process by using advanced analysis tools with high accuracy and to provide a robust model in support of cost-efficient monopile design especially in liquefiable sand.

2. SANISAND-MSu

The SANISAND-MS model (Liu et al., 2019) and SANISAND-MSu model (Liu et al., 2020) were formulated based on the framework of SANISAND2004. In these two models, some basic features of the SANISAND2004 model are preserved. The elastic domain is enclosed by a narrow conical yield surface in the stress ratio plane. Moreover, the critical state theory and state parameter concept (Been and Jefferies, 1985) are incorporated. Soil contractive/dilative behavior is distinguished by a phase transformation line (or the dilatancy surface in the stress ratio plane), which is defined through the critical state ratio and state parameter. The bounding surface plasticity theory is included in the model framework and is illustrated in the stress ratio plane as a wider conical cone. The bounding surface encloses the admissible stress states and is defined the same as the defemination to the phase transformation line through the evolving state parameter. The model follows the kinematic hardening rule and adopts the non-associated flow rule.

In contrast to SANISAND2004, the SANISAND-MS model (Liu et al., 2019) discards the concept of fabric tensor. Instead, an additional model surface, memory surface (MS), is adopted to phenomenologically capture the evolution of soil fabric during cyclic events and its influence on sand

plastic behavior (Liu and Pisanò, 2019). The memory surface is assumed to be in circular shape in cross-sections of the stress ratio plane (and conical in the stress ratio plane). The memory surface evolves upon plastic straining, both in size and location. The evolution of the memory surface should guarantee that the yield surface never goes out of the memory surface, and the memory surface size should never be smaller than the yield surface size.

Soil fabric effects are reflected in the hardening coefficient of the model formulations (thus, into the plastic modulus), through the evolution of the memory surface. Soil contractive behavior results in sand stiffening, which is linked to the increase in memory surface size. On the contrary, the dilative soil behavior causes a 'damage' to the soil fabric and usually leads to the decrease in soil stiffness enhancement. This phenomenon is translated into a shrinked memory surface.

The SANISAND-MSu model (Liu et al., 2020) furthers the success of SANISAND-MS with emphasis on the simulation of undrained cyclic behavior of sand. The improvements include: (1) incorporation of stress-ratio effects into the hardening coefficient to capture accurate cycle-by-cycle pore water pressure evolution before the stress state crosses the phase transformation line; and (2) a modified flow rule to properly capture the strain accumulation in cyclic mobility range.

Detailed SANISAND-MSu model equations and discussion can be found in Liu et al. (2020) and are not repeated here. The model performance in simulating cyclic triaxial tests on Kalsruhe fine sand (Wichtmann and Triantafyllidis, 2016) is given in Fig. 1. The sand has the following properties: a maximum void ratio of $e_{max} = 1.054$, a minimum void ratio of $e_{min} = 0.677$, a uniformity coefficient of $C_u = 1.5$, and a median particle diameter of $D_{50} = 0.14$ mm. The simulation conditions are defined undrained and as an initial effective confining pressure of $p_{in} = 200$ kPa, a cyclic deviator stress amplitude of $q_{ampl} = 45$ kPa, and an initial void ratio of $e_{in} = 0.81$.

The soil fabric (whose effects are simulated using the memory surface) and stress ratio effects on pore water pressure accumulation can be observed by noticing the required number of loading cycles to trigger the initial liquefaction (or to trigger the 'butterfly' shape stress path) when comparing Fig. 1(a) (SANISAND2004-based simulation results) with Fig. 1(c) (SANISAND-MSu-based simulation results). Without proper considerations of soil fabric and stress ratio effects prior to the initial liquefaction, the simulation results using SANISAND2004 underestimated the number of loading cycles to trigger cyclic mobility. Fig. 1(d) demonstrates that clear accumulation of axial strain on both positive and negative sides was captured by the SANISAND-MSu model, and the phenomenon agreed with the experimental observations. However, the simulation results in Fig. 1(b) using SANISAND2004 accumulated axial strain only on the negative side.

More validation evidence and model parameter calibration procedure can be found in Liu et al. (2020). To conclude, the SANISAND-MSu model was capable of simulating sand undrained cyclic behavior, and the sand fabric effects were well captured by the newly incorporated memory surface. The simulation results agreed with the experimental results. Therefore, the SANISAND-MSu model was believed to be a proper constitutive platform for finite element analysis of monopile cyclic behavior when pore water pressure effects were involved.

3. Simulation of pile lateral response using SANISAND-MSu

In this section, monopile behavior subjected to lateral loading was studied through an implicit 3D FE analysis

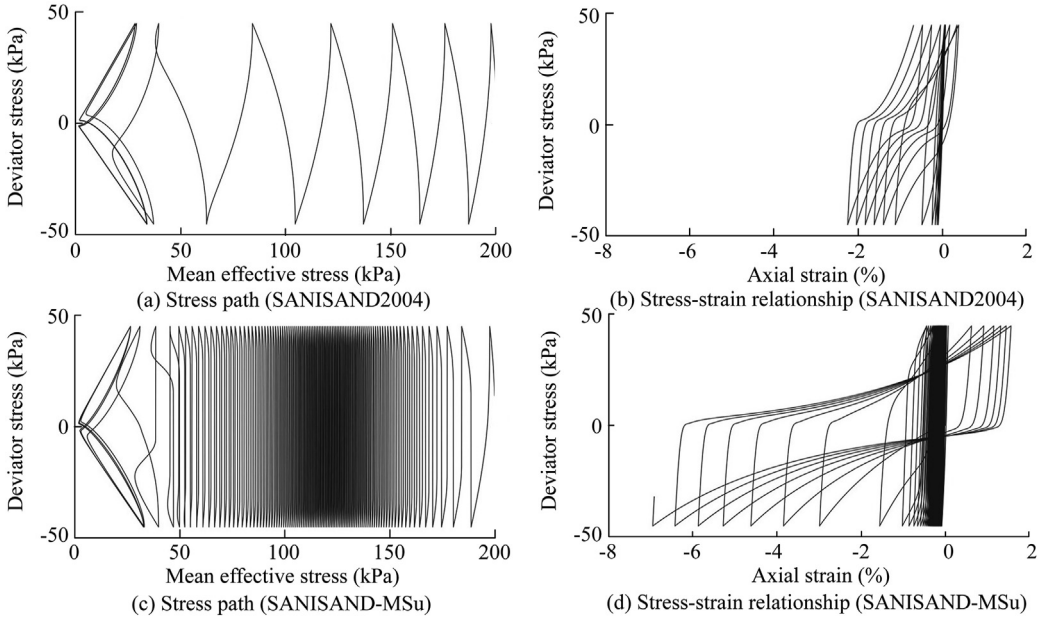

Fig. 1. Comparison between SANISAND-MSu and SANISAND2004 simulation results.

incorporating SANISAND-MSu. The open-source FE platform (OpenSEEs) was selected for this purpose. The same material (Karlsruhe fine sand) was used as the soil material. The model parameters were the same as those presented in Liu and Kaynia (2021). The 3D FE model is illustrated in Fig. 2. In total, 15 simulations were performed, including six push-over analyses and nine cyclic analyses. Pile geometry and soil drainage conditions for each test are summarized in Table 1. The aim of this section is to study the effect of pile geometry and static vertical load on monopile's lateral response. Comparison between the simulations under drained conditions and undrained conditions highlighted the role of the generated excess pore water pressure. The drainage condition in FE simulations was controlled by permeability. For drained cases, a permeability of $k = 10^{10}$ m/s was adopted; and for undrained cases, $k = 10^{-10}$ m/s. In all simulations in this study, the sand has a uniform relative density of $D_r = 80\%$.

Table 1
Summary of simulation cases.

Case	Loading type	L (m)	e (m)	Drainage type	Cyclic horizontal load (MN)	Vertical load (MN)
1	Monotonic	20	16	Drained		0
2	Monotonic	20	16	Undrained		0
3	Monotonic	20	16	Drained		6
4	Monotonic	20	16	Undrained		6
5	Monotonic	20	16	Drained		20
6	Monotonic	20	16	Undrained		20
7	Cyclic	30	18	Drained	12	0
8	Cyclic	30	18	Undrained	12	0
9	Cyclic	20	25	Undrained	12	0
10	Cyclic	25	25	Undrained	12	0
11	Cyclic	30	25	Undrained	12	0
12	Cyclic	25	18	Undrained	12	0
13	Cyclic	25	30	Undrained	12	0
14	Cyclic	30	30	Undrained	12	0
15	Cyclic	30	30	Undrained	12	6

3.1. Effects of drainage condition on lateral response

Push-over analyses of monopile were firstly investigated under both drained and undrained conditions for the simulation cases 1 and 2 (i.e., without static vertical load, pile geometries are indicated in Table 1). An ultimate limit state displacement of $y/D = 0.1$, where y is the pile displacement at the mudline, was adopted as the monopile failure criteria for the discussion of push-over analysis. The simulation results are presented in Fig. 3, which indicates that drainage condition had a clear effect on the monopile capacity. At monopile failure (i.e., $y/D = 0.1$), the estimated lateral capacity was around 55 MN in drained simulations, which was significantly smaller than that computed in undrained simulations (100 MN). Such a difference can be linked to the dilative behavior of sand at a shallow soil depth. Under undrained conditions, the excess pore water pressure reduced the mean effective stress p' in the soil. Such a decrease in p' promoted sand to enter the dilative zone if no load increment reversal was applied. It should be noted that whether monopile lateral capacity is larger in drained or undrained loading conditions depends highly on sand properties (Jostad et al., 2020).

Typical lateral load–displacement loops at the mudline are presented in Fig. 4. The pile has an embedded length of $L = 30$ m. A regular sinusoidal lateral cyclic loading with an amplitude of 12 MN was applied with an eccentricity of 18 m. The load was applied under both undrained and drained conditions (i.e., loading cases 7 and 8 in Table 1). No static vertical loading was considered. The load–displacement loop for the first loading cycle ($N = 1$) for undrained simulation (Fig. 4(a)) was similar to that of the drained simulation results (Fig. 4(b)). For a larger N, on the other hand, the accumulated displacement for each cycle under undrained conditions was much larger than the accumulated displacement under drained conditions. Obvious displacement accumulation was observed cycle-by-cycle for the undrained simulation. This was due to the significant soil degradation caused by the pore water pressure accumulation and stress redistribution. On the contrary, almost no displacement was accumulated within the number of loading cycles applied under drained conditions. The significant difference indicated that the traditional assumption of drained condition in monopile design in sand might be inaccurate if pore water pressure was generated and accumulated. This was also observed by Liu and Kaynia (2021).

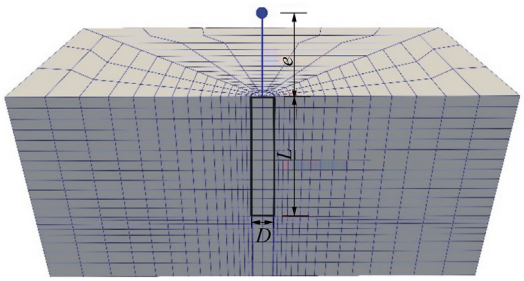

Fig. 2. 3D FE mesh used in OpenSEEs (L and e vary from case to case and D equals 5 m for all cases).

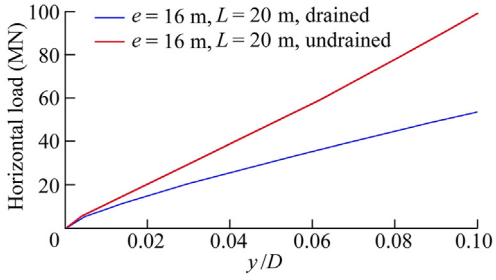

Fig. 3. Horizontal load against monopile pile displacement ratio (y/D) under both drained and undrained conditions.

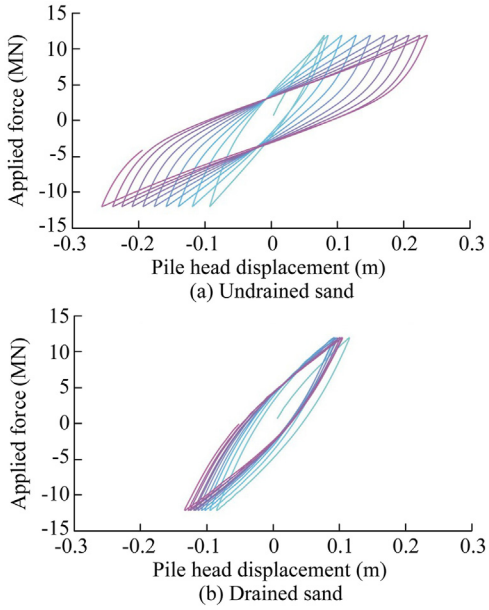

Fig. 4. Pile force displacement response in undrained and drained sand.

3.2. Effects of pile geometry on lateral response

In this section, the effect of pile geometry on the pile lateral response subjected to symmetric lateral sinusoidal loading is discussed. All simulations were performed under undrained conditions without applying static vertical load.

Pile head displacements (presented as y/D ratio) under varying L/D were studied through simulations using $L/D = 4$, 5, and 6 with corresponding embedded lengths of $L = 20$ m, 25 m, and 30 m, respectively. A load eccentricity of 25 m was used for all three cases (i.e., loading cases 9, 10, and 11 in Table 1). After eight loading cycles, pile head displacement was recorded when the applied load horizontal load H reached the maximum load level (i.e., $H = 12$ MN for all three cases). The simulation results are summarized in Fig. 5(a). As L/D ratios increased, the pile head displacement (or equivalently, y/D ratio) decreased linearly. A similar linear trend was reported in Jostad et al. (2020) for monotonic simulations under drained conditions using the hardening soil small strain model (Schanz et al., 1999) with an enhanced 3D FE analysis using Plaxis. However, the partially drained simulation results from the same work using the partially drained cyclic accumulation model (Jostad et al., 2015) suggested a non-linear decrease in pile head displacement with increasing L/D. The difference can be attributed to the monopile size, eccentricity, and loading type considered in the two studies. The effect of load eccentricity on pile's lateral displacement is schematically presented in Fig. 5(b). Pile head displacement (y/D ratio) increased linearly with e/D. In Fig. 5(b), all simulations were performed with a pile embedded length of $L = 25$ m (loading cases 12, 10, and 13 in Table 1 with corresponding e/D values of 3.6, 5.0, and 6.0, respectively).

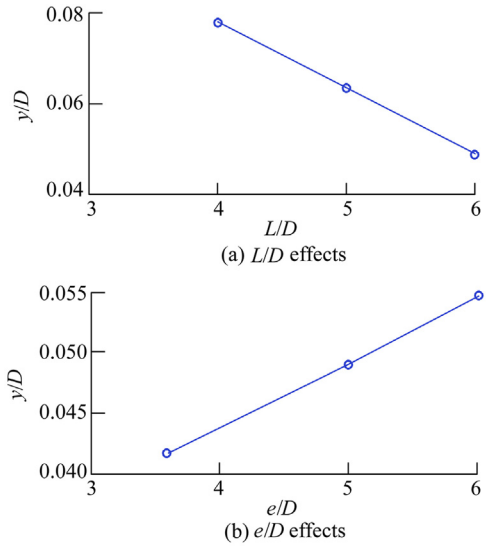

Fig. 5. Geometry effects on pile lateral displacement.

Fig. 6 presents the soil resistance (which was calculated as the integration of the shear force on the pile−soil interface) against pile deflection at different soil depths. Here pile deflection was defined as pile displacement along depth. The simulated monopile load eccentricity was 25 m. Different monopile embedded lengths ($L = 20$ m, 25 m, and 30 m) were considered (i.e., loading cases 9, 10, and 11 in Table 1). Due to the adopted different pile lengths, the compared soil reactions were not computed at the same absolute depth (z). Instead, they were recorded at the same relative depth normalized by the corresponding L (i.e., $z = 0.125L$ and $0.960L$).

At a shallow soil depth ($z = 0.125L$), soil reaction increased as the number of loading cycles increased. The loops for the simulations with different L presented the same shape but with different soil reaction levels at a given pile deflection level. Such an observation indicated that the L/D ratio had almost no effects on the pattern of soil reaction evolution. Only the magnitude of the soil reaction varied. As expected, the shorter the pile, the larger soil deformation was induced under the same load level at the same relative depth, thereby leading to greater soil reaction.

At a deep location ($z = 0.960L$), as L increased, soil reaction decreased at the same loading condition. This conclusion was the same as that obtained at a shallow soil depth. For a given L, soil reactions decreased with the number of loading cycles (N) at the investigated loading range. Such a conclusion was also found by Liu and Kaynia (2021), although loading was applied with zero eccentricity in the latter.

Similarly, the e/D effect on soil reaction is illustrated in Fig. 7, where the simulated monopiles had the same embedded length ($L = 30$ m). Loading eccentricity e varied from 18 m to 30 m (i.e., loading cases 12, 10, and 13 in Table 1). For different e/D ratios, soil reaction evolved in the same pattern: soil reaction at shallow soil depth increased as the number of

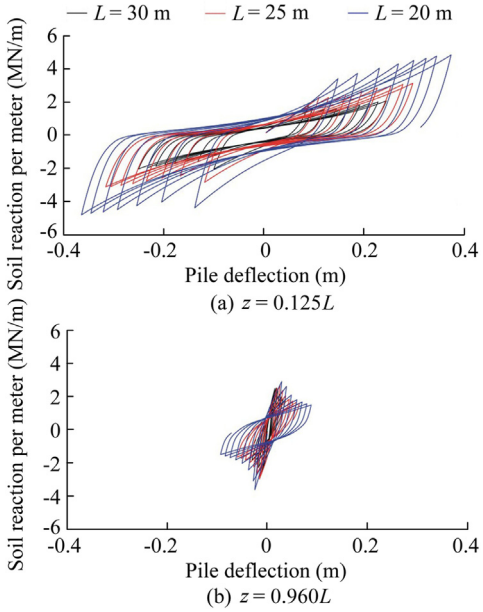

Fig. 6. Soil reaction against pile deflection.

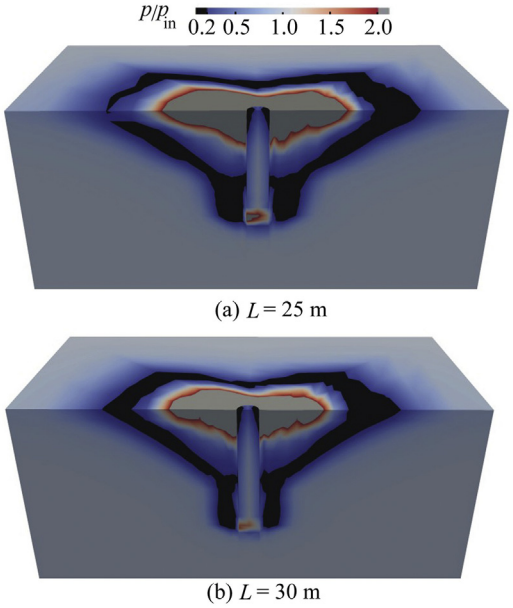

Fig. 8. Effective mean stress ratio distribution.

loading cycles increased; and soil reaction at deeper points first increased and then decreased as the number of loading cycles increased. At all soil depths, the magnitude of soil reaction at the same loading condition increased with the load eccentricity e.

Fig. 8 presents the distribution of p/p_{in} in the entire soil domain when the applied horizontal load H reached its peak value (12 MN) after eight loading cycles were applied. Horizontal load was applied at $e = 25$ m above the mudline. Two different embedded lengths ($L = 25$ m and 30 m) were considered. Overall, the p/p_{in} distributions were almost identical in the two simulation cases. Pile length had no significant effect on p/p_{in} ratios.

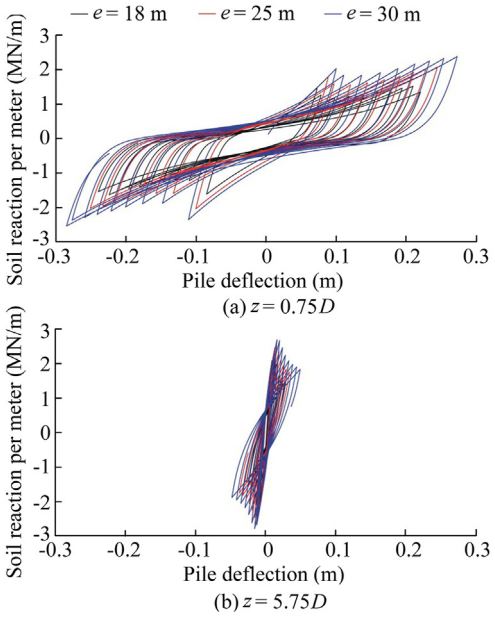

Fig. 7. Soil reaction against pile deflection.

To investigate in detail, p/p_{in} in all soil elements was initially equal to 1. After eight loading cycles, a clear increase in p/p_{in} was observed in both cases at shallow soil layers. This increase can be attributed to two reasons: (1) under undrained loading conditions, the shallow soil layers that had a small initial p_{in} entered the dilative zone at relatively large load levels; and (2) stress was redistributed during the cyclic loading event.

The increase in p/p_{in} at shallow soil layers near the monopile was in line with the increase of soil reaction as presented in Fig. 6(a). On the contrary, p/p_{in} decreased at larger depths around the monopile. Consequently, a reduced soil reaction was observed in Fig. 6(b) when the maximum soil reaction at $N = 1$ was compared with the maximum soil reaction at $N = 8$.

Fig. 9 displays the distribution of the excess pore water pressure in the entire soil domain for $H = 0$ after eight loading cycles were applied. The other simulation conditions were the same as the simulations presented in Fig. 8. For the two simulation cases with different embedded lengths, the maximum positive excess pore water pressure occurred at the pile tip. Negative pore water pressures can also be observed, mainly in the zone slightly below the pile tip and within the soil elements next to the pile head at shallow depths (close to the mudline). The distribution of excess pore water pressure above pile tip formed a wedge-like zone. In the case of $L = 25$ m, a wider distribution was observed with larger positive pore water pressures when comparing with the case of $L = 30$ m. Under the same loading condition (same horizontal

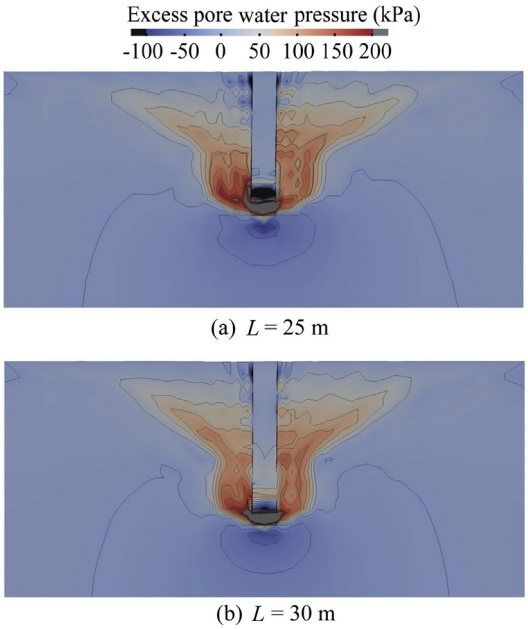

Fig. 9. Excess pore water pressure distribution.

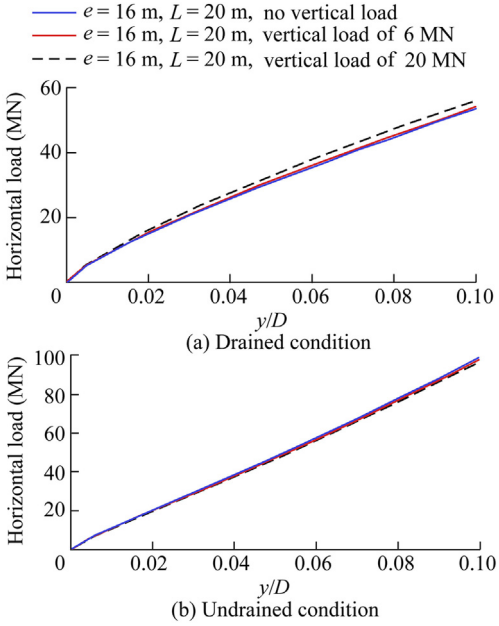

Fig. 10. Static vertical load effects on pile lateral capacity.

load and eccentricity), the shorter pile transformed a larger pressure to the surrounding soils. Therefore, larger amount of soil was mobilized to higher stress ratio levels. Under undrained cyclic conditions, this led to a larger positive pore water pressure accumulation if no significant dilative soil behavior was triggered.

4. Effect of static vertical load on monopile lateral response

Static vertical load applied on monopiles is usually due to the self-weight of the offshore wind turbine. The effect of static vertical load on monopile lateral behavior was studied in this work. Two cases were considered: (1) monotonic lateral loading and (2) cyclic lateral loading.

4.1. Monotonic lateral loading

The effect of static vertical load on lateral soil capacity was studied firstly through the push-over analysis. Both drained and undrained loading conditions were considered. The static vertical load of 6 MN is recognized as a representative load level for a typical 5-MW offshore wind turbine and was thus adopted as a typical static vertical load. The static vertical load of 20 MN was also studied for comparison. The loading cases are listed in Table 1 (loading cases 3−6). Lateral capacity of the monopile was defined as the applied horizontal load to cause $y/D = 0.1D$. The comparison is shown in Fig. 10. For the simulations with vertical static loading, about 15% of the gravity load was carried by the base, and the rest by skin friction.

For the drained case (Fig. 10(a)), only a small difference on monopile lateral capacity was observed when the simulation results with no vertical load were compared with those with a 6-MN vertical load within the monopile displacement range considered in this work. However, when the vertical load was increased to 20 MN, an obvious increase in monopile lateral capacity was observed. For the undrained case (Fig. 10(b)), vertical load showed minor effects on monopile lateral capacity, regardless of the static vertical load level.

4.2. Cyclic loading

The impact of static vertical load on monopile cyclic lateral response under undrained loading conditions was investigated in this section. Loading cases 14 and 15 (Table 1) were selected for such a study. The monopile has an embedded length of L = 30 m and an eccentricity of e = 30 m.

The load−displacement relationships for the simulation cases with and without a 6-MN static vertical load are presented in Fig. 11. Almost identical load displacement loops were obtained for $N \leq 2$. After that, pile head displacement was accumulated for the case with a 6-MN vertical load. However, the difference was minor within the investigated loading and displacement range.

Fig. 12 demonstrates the soil-reaction evolution with and without a 6-MN static vertical load, where the responses at two different depths ($z = 0.75D$ in Fig. 12(a) and $z = 5.75D$ in Fig. 12(b)) were considered. In align with the conclusion obtained from Fig. 11, the difference of soil-reaction evolution under the two different loading conditions was neglectable.

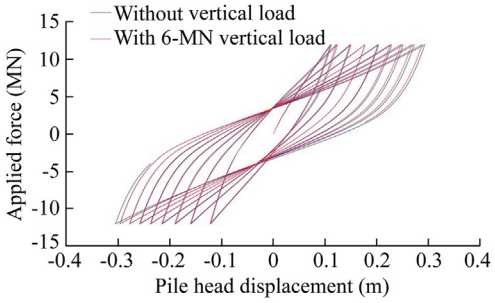

Fig. 11. Vertical load effects on monopile cyclic load−displacement relationship.

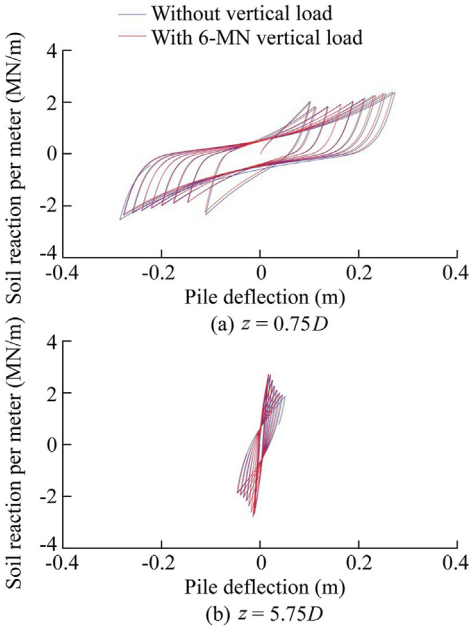

Fig. 12. Vertical load effects on soil reaction−pile deflection relationship.

5. Conclusions

In this work, the implicit cyclic material model SANISAND-MSu was firstly presented. Model features were presented through model simulations against undrained cyclic triaxial tests in sand. The effects of pore water pressure on monopile lateral behavior were discussed using the SANISAND-MSu model by an enhanced 3D FE analysis method. Both monotonic loading and cyclic loading conditions were considered. Compared to the drained simulation result, an increasing lateral capacity was obtained for the investigated soil material in undrained simulation under monotonic loading. For undrained cyclic loading conditions, significant cycle-by-cycle pile lateral displacement was developed. In drained cases, the evolving of monopile displacement from cycle to cycle was less obvious.

Further, the effects of monopile geometry on the monopile lateral behavior under undrained loading conditions were studied. Within the loading and geometry range predefined in this work, the accumulated pile head displacement decreased linearly with the L/D ratio but increased with e/D. Soil response was then studied from the effective stress (p/p_{in}) distribution and pore water pressure distribution viewpoints.

The static vertical load applied in this work (6 MN) had negligible effects on the pile lateral response, both with regards to the lateral push-over capacity (study based on monopiles with $D = 5$ m, $L = 20$ m, and $e = 16$ m) and cyclic load−displacement response and cyclic soil reaction evolution perspective (study based on monopiles with $D = 5$ m, $L = 30$ m, and $e = 30$ m).

The results in this work aimed to raise attention to considering the soil drainage condition and role of excess pore water pressure in optimized monopile design. The discussion on the effect of pile geometry and static vertical load was considered to provide guidance to the simple estimation on monopile lateral behavior.

Declaration of competing interest

The authors declare no conflicts of interest.

References

API, 2014. Recommended Practice 2AWSD Planning, Designing and Constructing Fixed Offshore Platforms − Working Stress Design, 22nd Edition. American Petroleum Institute, Washington, D.C.

Been, K., Jefferies, M.G., 1985. A state parameter for sands. Geotechnique 35(2), 99−112. https://doi.org/10.1680/geot.1985.35.2.99.

Dafalias, Y.F., Popov, E.P., 1975. A model of nonlinearly hardening materials for complex loading. Acta Mech. 21(3), 173−192. https://doi.org/10.1007/BF01181053.

Dafalias, Y.F., Manzari, M.T., 2004. Simple plasticity sand model accounting for fabric change effects. J. Eng. Mech. 130(6), 622−634. https://doi.org/10.1061/(ASCE)0733-9399(2004)130:6(622).

Esfeh, P.K., Kaynia, A.M., 2020. Earthquake response of monopiles and caissons for offshore wind turbines founded in liquefiable soil. Soil Dynam. Earthq. Eng. 136, 106213. https://doi.org/10.1016/j.soildyn.2020.106213.

Houlsby, G.T., Abadie, C.N., Beuckelaers, W.J.A.P., Byrne, B.W., 2017. A model for nonlinear hysteretic and ratcheting behaviour. Int. J. Solid Struct. 120, 67−80. https://doi.org/10.1016/j.ijsolstr.2017.04.031.

Jostad, H., Grimstad, G., Andersen, K., Sivasithamparam, N., 2015. A FE procedure for calculation of cyclic behaviour of offshore foundations under partly drained conditions. Frontiers in Offshore Geotechnics III 1, 153−172. https://doi.org/10.1201/b18442-9.

Jostad, H.P., Dahl, B.M., Page, A., Sivasithamparam, N., Sturm, H., 2020. Evaluation of soil models for improved design of offshore wind turbine foundations in dense sand. Geotechnique 70(8), 682−699. https://doi.org/10.1680/jgeot.19.TI.034.

Kaynia, A.M., 2019. Seismic considerations in design of offshore win turbines. Soil Dynam. Earthq. Eng. 124, 399−407. https://doi.org/10.1016/j.soildyn.2018.04.038.

Klinkvort, R.T., 2013. Centrifuge Modelling of Drained Lateral Pile−Soil Response: Application for Offshore Wind Turbine Support Structures. Ph. D. Dissertation. Technical University of Denmark, Copenhagen.

Krieg, R.D., 1975. A practical two surface plasticity theory. J. Appl. Mech. 42(3), 641−646. https://doi.org/10.1115/1.3423656.

LeBlanc, C., Houlsby, G.T., Byrne, B.W., 2010. Response of stiff piles in sand to long-term cyclic lateral loading. Geotechnique 60(2), 79−90. https://doi.org/10.1680/geot.7.00196.

Liu, H.Y., Abell, J.A., Diambra, A., Pisanò, F., 2019. Modelling the cyclic ratcheting of sands through memory-enhanced bounding surface plasticity. Geotechnique 69(9), 783−800. https://doi.org/10.1680/jgeot.17.P.307.

Liu, H.Y., Pisanò, F., 2019. Prediction of oedometer terminal densities through a memory-enhanced cyclic model for sand. Géotech. Lett. 9(2), 81−88. https://doi.org/10.1680/jgele.18.00187.

Liu, H.Y., Diambra, A., Abell, J.A., Pisanò, F., 2020. Memory-enhanced plasticity modeling of sand behavior under undrained cyclic loading. Journal of Geotechnical and Geoenvironmental Engineering 146(11), 04020122. https://doi.org/10.1061/(ASCE)GT.1943-5606.0002362.

Liu, H.Y., Kaynia, A.M., 2021. Cyclic undrained behaviour of SANISAND-MS and its effects on response of monopiles for offshore wind structures. Geotechnique. https://doi.org/10.1680/jgeot.21.00068.

Liu, H.Y., Kementzetzidis, E., Abell, J.A., Pisanò, F., 2021. From cyclic sand ratcheting to tilt accumulation of offshore monopiles: 3D FE modelling using SANISAND-MS. Geotechnique. https://doi.org/10.1680/jgeot.20.P.029.

Mróz, Z., 1967. On the description of anisotropic work hardening. J. Mech. Phys. Solid. 15(3), 163−175. https://doi.org/10.1016/0022-5096(67)90030-0.

Niemunis, A., Wichtmann, T., Triantafyllidis, T., 2005. A high-cycle accumulation model for sand. Comput. Geotech. 32(4), 245−263. https://doi.org/10.1016/j.compgeo.2005.03.002.

Page, A.M., Grimstad, G., Eiksund, G.R., Jostad, H.P., 2019. A macro-element model for multidirectional cyclic lateral loading of monopiles in clay. Comput. Geotech. 106, 314−326. https://doi.org/10.1016/j.compgeo.2018.11.007.

Richards, I.A., Byrne, B.W., Houlsby, G.T., 2020. Monopile rotation under complex cyclic lateral loading in sand. Geotechnique 70(10), 916−930. https://doi.org/10.1680/jgeot.18.P.302.

Schanz, T., Vermeer, P.A., Bonnier, P.G., 1999. The hardening soil model: Formulation and verification. In: Brinkgeve, R.B.J. (Ed.), Beyond 2000 in Computational Geotechnics − 10 Years of PLAXIS. Balkema, Rotterdam, pp. 281−296.

Staubach, P., Wichtmann, T., 2020. Long-term deformations of monopile foundations for offshore wind turbines studied with a high-cycle accumulation model. Comput. Geotech. 124, 103553. https://doi.org/10.1016/j.compgeo.2020.103553.

Tasiopoulou, P., Chaloulos, Y., Gerolymos, N., Giannakou, A., Chacko, J., 2021. Cyclic lateral response of OWT bucket foundations in sand: 3D coupled effective stress analysis with Ta-Ger model. Soils Found. 61(2), 371−385. https://doi.org/10.1016/j.sandf.2020.12.002.

Truong, P., Lehane, B.M., Zania, V., Klinkvort, R.T., 2019. Empirical approach based on centrifuge testing for cyclic deformations of laterally loaded piles in sand. Geotechnique 69(2), 133−145. https://doi.org/10.1680/jgeot.17.P.203.

Wichtmann, T., Triantafyllidis, T., 2016. An experimental database for the development, calibration and verification of constitutive models for sand with focus to cyclic loading: Part I − tests with monotonic loading and stress cycles. Acta Geotechnica 11(4), 739−761. https://doi.org/10.1007/s11440-015-0402-z.